On the Mechanism of Hydrogen Transfer in the HSCH(O) ⇌ (S)CHOH and HSNO ⇌ SNOH Reactions

Soledad Gutiérrez-Oliva,[†] Bárbara Herrera,[‡] Alejandro Toro-Labbé,*[,‡] and Henry Chermette[§]

Centro de Bioinformática y Simulación Molecular, Universidad de Talca, Casilla 721, Talca, Chile, Laboratorio de Química Teórica Computacional, Facultad de Química, Pontificia Universidad Católica de Chile, Casilla 306, Correo 22, Santiago 6094411, Chile, and Laboratoire de Chimie Physique Théorique, Université Claude Bernard Lyon-1 and UMR CNRS 5182, Villeurbanne Cedex 69622, France

Received: October 15, 2004; In Final Form: December 5, 2004

The 1,3-intramolecular hydrogen transfer in the HSCH(O) ⇌ (S)CHOH and HSNO ⇌ SNOH reactions is studied through density functional theory calculations. The reaction force together with structural and electronic properties is monitored along the reaction path to characterize the mechanism of hydrogen transfer. It is found that in both reactions the hydrogen transfer is activated by the structural rearrangement of the backbone atoms that allow the electrostatic interactions to promote the hydrogen transfer in a stepwise mechanism.

1. Introduction

Hydrogen bonds are attractive weak interactions between a polar bond, usually CH, NH, OH, or SH, and a polar neighboring atom bearing a negative charge.[1−4] Hydrogen transfer may thus occur between the donor atom (**D**) that is bonded to the hydrogen (**D**−H) and a near neighbor acceptor atom (**A**) that is hydrogen bonded with the **D**−H moiety.[5−9] In this paper, a study of the hydrogen-transfer reaction **D**−H···**A** → **D** ···H−**A**, where **D** and **A** are oxygen and sulfur atoms, is presented. The main goal of this work is to characterize the mechanism of hydrogen transfer in HSCH(O) ⇌ (S)CHOH (**R1**) and HSNO → SNOH (**R2**), as shown in Figure 1.

Characterization of the mechanisms that activate the intramolecular hydrogen transfer can be achieved by monitoring the energy and the reaction force profiles during the process; their critical points along the reaction coordinate help identify the different mechanisms that operate during the transfer. The energy profile along a reaction path not only gives information about kinetics and thermodynamics properties of the reaction but also about the reaction mechanism.[10,11] Part of this information can be obtained from the reaction force profile, the derivative of the energy profile, and the simultaneous analysis of structural and electronic properties such as bond distances and angles, electronic populations and dipole moments. The profile of the reaction force leads to the definition of different regions along the reaction coordinate[10−13] in which different reaction mechanisms might be operating. To each of these regions there are associated specific amounts of work that are calculated by integrating the force profile within the specific region, this allows the quantification of the energy cost of each step of the reaction.

This paper is organized as follows: in section 2 we present the conceptual frame that characterizes the different regions along the reaction coordinate. Section 3 is devoted to the computational details, and in section 4, we present and discuss the results; section 5 contains our concluding remarks.

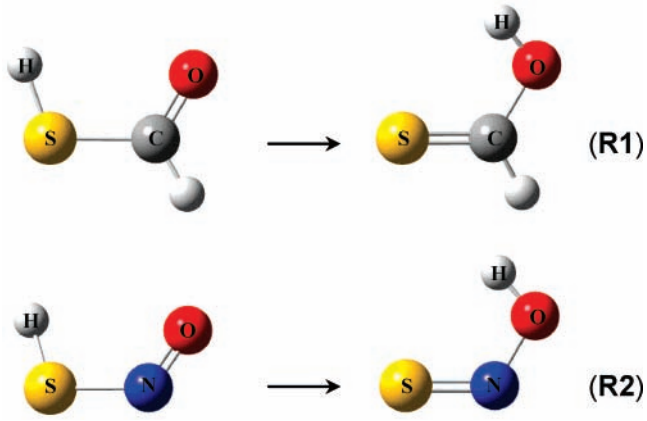

Figure 1. Sketch of the HSCH(O) ⇌ (S)CHOH (**R1**) and HSNO ⇌ SNOH (**R2**) hydrogen-transfer reactions.

2. Energy and Force Profiles

A chemical reaction occurs through the simultaneous change of different geometrical parameters in a multidimensional space. This multidimensional motion is condensed to ω, the intrinsic reaction coordinate (IRC), such that the energy profile along ω, $E(\omega)$, is the lowest energy path relaying reactants to products. Numerical differentiation of $E(\omega)$ leads to the Hellmann−Feynman reaction force[10,12,13]

$$F(\omega) = -\frac{dE(\omega)}{d\omega} \tag{1}$$

This is a global property of the reaction that contains all the information concerning the specific interactions that drive the reaction from reactants to products, although in most cases this information is hardly available since the multidimensional reaction coordinate is yet unknown. However, $F(\omega)$ provides the elements to characterize the different reaction mechanisms that might be operating along the reaction coordinate. As the derivative of the energy profile, $F(\omega)$ present two critical points,

* Author to whom correspondence may be addressed. E-mail: atola@puc.cl.
[†] Universidad de Talca.
[‡] Pontificia Universidad Católica de Chile.
[§] Université Claude Bernard.

10.1021/jp0452756 CCC: $30.25
Published on Web 02/04/2005

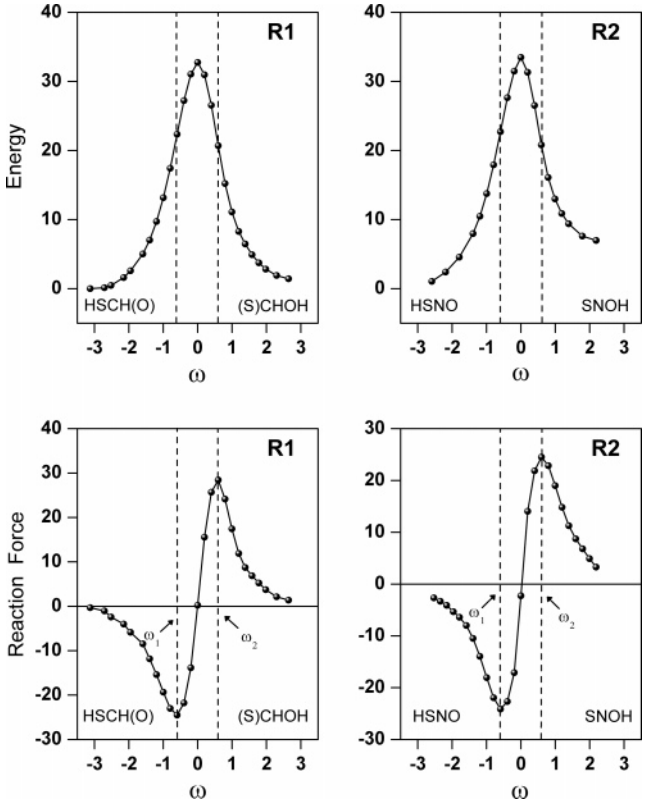

Figure 2. Relative energy (in kcal/mol) and chemical force profiles (in kcal/mol·ω) of **R1** and **R2**. The dashed vertical lines indicate the limits of the different regions identified along the reaction coordinate.

at ω_1 and ω_2; these points are the inflection points of the energy profile and define different regions along ω where different kind of processes take place, see Figure 2.

The reactants region is defined within the interval $-\infty \leq \omega \leq \omega_1$, where the chemical species are expected to present most characteristics of the reactants and begin to be activated to reach the transition state (TS) region. The TS region is defined within the interval $\omega_1 < \omega < \omega_2$, in this region the chemical species define their unique TS structure to pursuing the reaction. Finally the product region is defined within the interval $\omega_2 \leq \omega \leq \infty$ where the system relaxes to reach the product. The first step of the reaction requires an amount of work $W_1 = -\int_{-\infty}^{\omega 1} F(\omega)\, d\omega$, necessary to bring the donor and acceptor atoms as close as possible to each other to activate the hydrogen transfer.[11,13] The work that is necessary to reach the TS from ω_1 is $W_2 = -\int_{\omega 1}^{0} F(\omega)\, d\omega$, which is usually smaller than W_1.[11−13] Note that $W_1 + W_2$ is equal to the energy barrier $\Delta E^{\neq}$.

3. Computational Details

Calculations along the reaction coordinate were performed at the B3LYP/6-311G** level of theory.[14,15] The reaction path followed by the hydrogen atom from the donor atom to the acceptor atom passing by the transition state always lied in the molecular plane. The profiles of energy, force, bond distances and angles as well as Mulliken populations and dipole moments were obtained through single-point calculations on the previously optimized geometries given by the IRC procedure.[16] All calculations were performed using the *Gaussian 98/03* packages.[17,18]

4. Results and Discussion

4.1. Energy and Force Profiles. The energy and force profiles along the intrinsic reaction coordinate of **R1** and **R2** are shown in Figure 2, and the energetic parameters are displayed in Table 1. It is remarkable that the values of $\Delta E°$ associated with the **R2** reaction are about five times those of **R1**. Both reactions are endoenergetic, indicating that the oxygen atom makes a stronger hydrogen bond in the reactant structure than does the sulfur in the product. On the other hand, since the barriers for the hydrogen transfer of the direct reactions are higher than that of the reverse reactions, the donor−acceptor couple sulfur−oxygen of the reactants is not as good as the oxygen−sulfur couple of the reverse reactions. In fact, it is well-known that oxygen is a better hydrogen acceptor and a worse hydrogen donor than sulfur; barrier heights seems to say the contrary. However, since the energy barriers take into account different specific interactions that are activated at different steps as the reaction goes by, they are not only determined by the relative hydrogen donor−acceptor power of sulfur and oxygen atoms but also by contributions associated to the initial structural rearrangement necessary to activate the hydrogen transfer. Once the transfer is activated by the structural motion, the donor and acceptor capabilities of the involved atoms start to play a role to achieve the transfer.

TABLE 1: DFT/B3LYP//6-311G Reaction Energy ($\Delta E°$), Energy Barrier ($\Delta E^{\neq}$), Work Performed by the System during the Structural Rearrangement (W_1), and the Work Necessary to Bring the Hydrogen at the Transition State (W_2) for the Two Hydrogen Transfers R1 and R2 (All Values Are in kcal/mol)**

reaction	$\Delta E°$	$\Delta E^{\neq}$	W_1	W_2
HSCH(O) ⇌ (S)CHOH (R1)	1.43	32.75	22.35	10.40
HSNO ⇌ SNOH (R2)	6.99	33.48	22.72	10.76

Also displayed in Figure 2 are the reaction forces associated to both reactions. The minimum and maximum of the force profiles are indicated by the vertical dashed lines that are also displayed in the profiles of energy and forthcoming properties. The regions defined by a $F(\omega)$ are specific regions in which different steps of the reaction mechanism operates; at the reactant region, the backbone structural rearrangement activate the reaction, and the work required for this process that brings the donor and acceptor atoms closer to each other is $W_1 = -\int_{-\infty}^{\omega 1} F(\omega)\, d\omega$. From ω_1, the work necessary to reach the transition state is $W_2 = -\int_{\omega 1}^{0} F(\omega)\, d\omega$. Note that during the activation process occurring within the whole interval $-\infty \leq \omega \leq 0$ the energy of the system increases and therefore the work is positive and it is assumed to be done on the system by the surroundings. In this way, a quantitative approach to the reaction mechanism is obtained through the analysis of the reaction force profiles. The values of W_1 and W_2 ($W_1 + W_2 = \Delta E^{\neq}$) are displayed in Table 1, it is interesting to note that these quantities for **R1** and **R2** are quite close, thus stressing the similarity of both reactions.

Within the reactant region, the donor and acceptor power of the atoms are not playing an important role to promote the hydrogen transfer; it is only at the TS region where the power of the donor and acceptor atoms drives the hydrogenic motion, note that in both reactions the energy barrier involved only in this step, i.e., from ω_1 to 0, is smaller than the one associated to the reverse reaction thus confirming the expected result: oxygen is a better hydrogen acceptor than sulfur. The barrier when going from ω_2 to 0 in the reverse reactions shows that oxygen is a worse hydrogen donor than sulfur because the OH bond is stronger than the SH bond. These results are in agreement with what is expected from chemical grounds.

It is interesting to note that in the two cases the overall reaction is determined by the first step in which the backbone

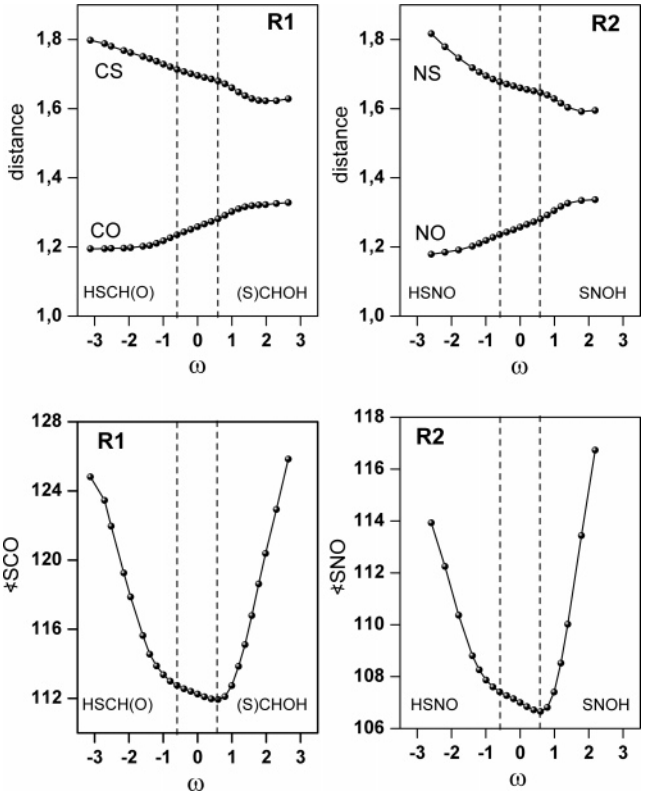

Figure 3. Backbone bond distances and angles profiles (in angstroms and degrees) of **R1** and **R2**.

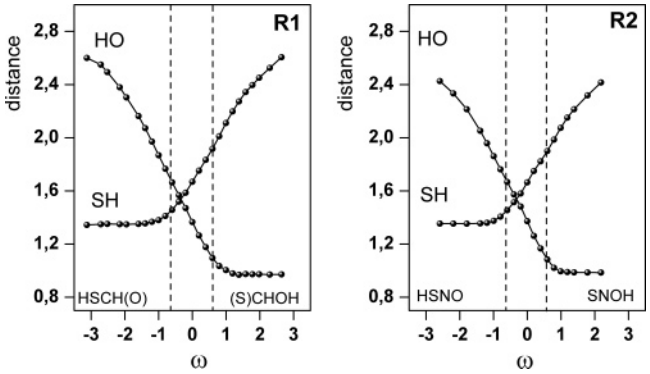

Figure 4. Profiles of the distances (in angstroms) between the moving hydrogen and the donor and acceptor atoms.

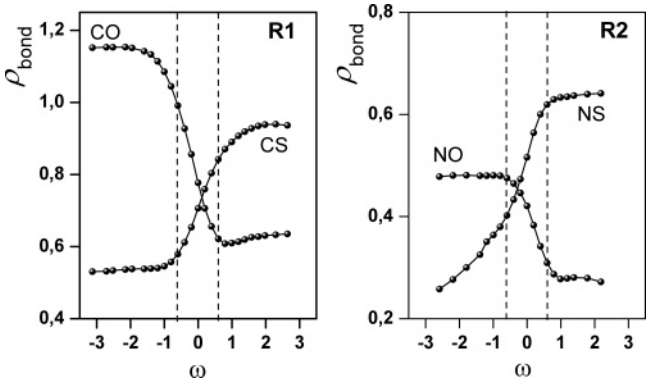

Figure 5. Profiles of the backbone bond populations involving the donor and acceptor atoms in **R1** and **R2**. All values are in au.

motion brings the donor and acceptor atoms near to each other in order to allow the subsequent hydrogen transfer. In other words, the transfer is activated if and only if the donor and acceptor atoms arrange themselves to be in the right position to promote the transfer. The energy needed to produce this structural rearrangement is W_1, and it is quite similar in both reactions. The $W_3 = -\int_0^{\omega 2} F(\omega)\, d\omega$ and $W_4 = -\int_{\infty}^{\omega 2} F(\omega)\, d\omega$ may be used in a similar way to interpret the reverse reaction.

4.2. Structural Rearrangement. When comparing the evolution along ω of the backbone bond distances and angles that are displayed in Figure 3, we note quite similar trends in both reactions. The bond distances CO (**R1**) and NO (**R2**) increase monotonically, whereas the bond distances CS (**R1**) and NS (**R2**) decrease monotonically when going from reactants to products. This is due in the first case (CO and NO) to the loss of double-bond character and in the second case (CS and NS) to the gain of double-bond character. The overall small changes of the backbone bond distances along ω indicate that these are quite inactive modes in promoting the hydrogen transfer.

On the other hand, when analyzing the evolution of the SCO angle in **R1** and the SNO angle in **R2**, it becomes evident that these are the reactive modes that activate the hydrogen transfer. In the reactant regions, these angles decrease drastically allowing the donor and acceptor atoms to get closer to each other thus activating the transfer; the energetic cost associated is W_1 and in both reactions is about 22 kcal/ mol, see Table 1. Within the **TS** region, the bond angles change slightly to allow the hydrogenic motion, then at the product region the structural relaxation causes them to increase sharply to reach the equilibrium value of the product molecule. The relatively small variation of the SNO angle in **R2** with respect to SCO in **R1** indicates that the system involved in **R2** is somewhat more rigid than the one involved in **R1**.

Figure 4 displays the variation of the distances **D**−H and H−**A** between the donor (S) and acceptor (O) atoms with the hydrogen being transferred along the reaction coordinate in **R1** and **R2**, respectively. Note that the H−**A** distances decrease monotonically from reactants to the product region's limit at ω_2, thereafter they remain constant. Interestingly in the reactant region the **D**−H distance remains practically constant, therefore the shortening of the H−**A** distance is basically due to the decrease in the backbone bond angles and not to the motion of the hydrogen itself. Clearly the hydrogenic motion practically starts at ω_1 and ceases in ω_2.

4.3. Bond Electronic Populations. The precedent discussion indicates that activation and relaxation processes should be characterized by specific interactions; these can be identified through the simultaneous analysis of the reaction force and local electronic populations.[11−13] Profiles of specific Mulliken's bond populations (ρ_{bond}) along the reaction coordinate are shown in Figure 5.

Note that at the reactant and product regions of **R1** all populations remain quite constant, but when they enter the TS region, they vary sharply, drastically changing their values. The most noticeable changes of the population associated to bonds of the donor and acceptor atoms with the adjacent carbon (CO and CS) occur at the vicinity of ω_1. The CO and CS bond populations cross each other at the TS, indicating that a maximum electronic delocalization is reached at this point. Clearly delocalization is not required to activate the structural rearrangement; it shows up only when the hydrogenic motion is well advanced. On the other hand, it is interesting to notice that CO and CS electronic populations are closer to each other in the product region than in the reactant region, indicating that in some extent delocalization is stabilizing the product molecule in **R1** thus leading to a quite small $\Delta E°$ value, as shown in Table 1.

At the reactant and product regions of **R2**, all bond populations are quite constant except the NS population that, at the

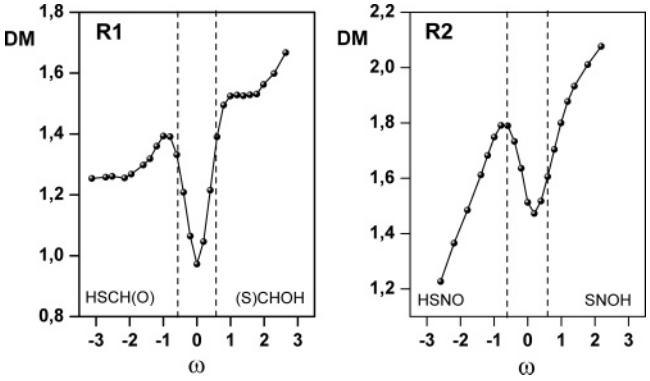

Figure 6. Profiles of the dipole moments (in Debye) of **R1** and **R2**.

reactant region, increases, indicating some extent of hyperconjugation along the SNO unit probably involving the lone pairs of the three atoms, this is in agreement with the already observed rigidity of the SNO group in **R2** in comparison with SCO of **R1**. Moreover, in contrast to **R1**, the difference between the NO and NS populations is smaller in the reactant region than in the product one, here the electronic delocalization seems to be stabilizing the reactant molecule. The opposite behavior of delocalization in **R1** and **R2** may explain the large difference between the reaction energies. Again the NO and NS populations cross each other at the TS region, indicating that the TS structure is characterized by the highest degree of delocalization among the backbone atoms.

In summary, when the hydrogen is transferred, after that the structural rearrangement process take place, ρ_{D-H} decreases, whereas ρ_{D-A} increases. The overall change of the bond populations of donor and acceptor atoms with the adjacent nitrogen in **R2** is smaller than the changes observed in the CO and CS populations of **R1**. This indicates that **R1** occurs with a larger redistribution of the electronic density than **R2**.

4.4. Dipole Moment. Figure 6 shows the evolution of the dipole moment (DM) that reflects the internal charge separation during the hydrogen transfer. In general, both reactions present a similar trend with a sharp minimum at the TS. In **R1**, the backbone motion that occurs in the reactant region leaves the DM quite constant, helped by the small electronic density reordering observed in this region. The maximum change of DM observed in the reactant region is quite small, about 0.2 D, indicating again that the structural rearrangement is not producing noticeable changes in the electronic density; this is in agreement with the already discussed behavior of bond populations. In the product region, the DM is a little larger than in the reactant region, basically due to the structural differences between the two systems. The minimum at the TS is consistent with the maximum electronic delocalization indicated in Figure 5 by the crossing of the CS and CO populations.

At the reactant region of **R2**, the rearrangement of the backbone structure produces a monotonic increase of the dipole moment by about 0.6 D to reach a maximum at ω_1. Then it goes down at the transition state region reaching a minimum at the TS, in agreement with the maximum electronic delocalization observed in the analysis of electronic populations. In the product region, the structural relaxation drives the DM to its final maximum value as the product structure is attained.

5. Concluding Remarks

In light of the above results, one may speculate that these hydrogen transfers proceed roughly as follows: the initial phase for both reactions is essentially a structural rearrangement driven by a bending motion of the **D**X**A** angle (X = C in **R1** and X = N in **R2**) that bring the donor and acceptor atoms as close together as possible. At a certain point ω_1, when the structural rearrangement practically ceases, the growing attraction of the proton to the electronic charge of the acceptor drives the hydrogen transfer. Eventually the process arrives at a point ω_2 corresponding basically to a stretched H−**A** with a bent backbone structure; thereafter the driving force toward the equilibrium product structure decreases as the bond becomes shorter and bending angle becomes larger to finally reach the products of the reactions.

Acknowledgment. This work was initiated during a sabbatical stay of A.T.L. at the Claude Bernard University in Lyon, France. The CINES (France) is acknowledged for a grant of computer time. Financial support from FONDECYT through Project No. 1020534 and MECESUP through Projects PUC-0004 and Red Química UCH-0116 are acknowledged. B.H. wishes to thank CONICYT for Doctoral and Termino de Tesis fellows. S.G.-O. acknowledges financial support from Nucleo Milenio de Mecanica Cuantica Aplicada y Quimica Computacional, Codigo P02-004-F.

References and Notes

(1) Jeffrey, G. A.; Saenger, W. *Hydrogen Bonding in Biological Structures*; Springer-Verlag: Berlin, Germany, 1991.
(2) Scheiner, S. *Hydrogen Bonding: a Theoretical Perspective*; Oxford University Press: New York, 1997.
(3) Klaholz, B. P.; Mitschler, A.; Moras, D. *J. Mol. Biol.* **2000**, *302*, 155.
(4) Desiraju, G. R.; Steiner, T. *In The Weak Hydrogen Bond in Structural Chemistry and Biology*; Oxford University Press: New York, 1999; Vol. 9.
(5) Wennmohs, F.; Staemmler, V.; Schindler, M. *J. Chem. Phys.* **2003**, *119*, 3208.
(6) Löwdin, P. O. R. *Mod. Phys.* **1963**, *35*, 724.
(7) Voet, D.; Voet, J. G. *Biochemistry*; John Wiley and Sons: New York, 1995.
(8) Sevilla, M. D.; Besler, B.; Colson, A. O. *J. Phys. Chem.* **1995**, *99*, 1060.
(9) Jensen, J. H.; Gordon, M. S. *J. Am. Chem. Soc.* **1995**, *117*, 8159.
(10) Toro-Labbé, A. *J. Phys. Chem. A* **1999**, *103*, 4398.
(11) Jaque, P.; Toro-Labbé, A. *J. Phys. Chem. A* **2000**, *104*, 995.
(12) Toro-Labbé, A.; Gutiérrez-Oliva, S.; Concha, M. C.; Murray, J.; Politzer, P. *J. Chem. Phys.* **2004**, *121*, 4570.
(13) Herrera, B.; Toro-Labbé, A. *J. Chem. Phys.* **2004**, *121*, 7096.
(14) Becke, A. D. *J. Chem. Phys.* **1993**, *98*, 5648.
(15) Lee, C.; Yang, W.; Parr, R. G. *Phys. Rev.* **1988**, *37*, 785.
(16) Fukui, K. *Acc. Chem. Res.* **1981**, *14*, 363.
(17) Frisch, J. M.; Trucks, G. W.; Schlegel, H. B.; Scuseria, G. E.; Robb, M. A.; Cheeseman, J. R.; Zakrzewski, V. G.; Montgomery, J. A., Jr.; Stratmann, R. E.; Burant, J. C.; Dapprich, S.; Millam, J. M.; Daniels, A. D.; Kudin, K. N.; Strain, M. C.; Farkas, O.; Tomasi, J.; Barone, V.; Cossi, M.; Cammi, R.; Mennucci, B.; Pomelli, C.; Adamo, C.; Clifford, S.; Ochterski, J.; Petersson, G. A.; Ayala, P. Y.; Cui, Q.; Morokuma, K.; Malick, D. K.; Rabuck, A. D.; Raghavachari, K.; Foresman, J. B.; Cioslowski, J.; Ortiz, J. V.; Baboul, A. G.; Stefanov, B. B.; Liu, G.; Liashenko, A.; Piskorz, P.; Komaromi, I.; Gomperts, R.; Martin, R. L.; Fox, D. J.; Keith, T.; Al-Laham, M. A.; Peng, C. Y.; Nanayakkara, A.; Gonzalez, C.; Challacombe, M.; Gill, P. M. W.; Johnson, B.; Chen, W.; Wong, M. W.; Andres, J. L.; Gonzalez, C.; Head-Gordon, M.; Replogle, E. S.; Pople, J. A. 1998.
(18) Frisch, M. J.; Trucks, G. W.; Schlegel, H. B.; Scuseria, G. E.; Robb, M.A.; Cheeseman, J. R.; Montgomery, J. A., Jr.; Vreven, T.; Kudin, K. N.; Burant, J. C.; Millam, J. M.; Iyengar, S. S.; Tomasi, J.; Barone, V.; Mennucci, B.; Cossi, M.; Scalmani, G.; Rega, N.; Petersson, G. A.; Nakatsuji, H.; Hada, M.; Ehara, M.; Toyota, K.; Fukuda, R.; Hasegawa, J.; Ishida, M.; Nakajima, T.; Honda, Y.; Kitao, O.; Nakai, H.; Klene, M.; Li, X.; Knox, J. E.; Hratchian, H. P.; Cross, J. B.; Adamo, C.; Jaramillo, J.; Gomperts, R.; Stratmann, R. E.; Yazyev, O.; Austin, A. J.; Cammi, R.; Pomelli, C.; Ochterski, J. W.; Ayala, P. Y.; Morokuma, K.; Voth, G. A.; Salvador, P.; Dannenberg, J. J.; Zakrzewski, V. G.; Dapprich, S.; Daniels, A. D.; Strain, M. C.; Farkas, O.; Malick, D. K.; Rabuck, A. D.; Raghavachari, K.; Foresman, J. B.; Ortiz, J. V.; Cui, Q.; Baboul, A. G.; Clifford, S.; Cioslowski, J.; Stefanov, B. B.; Liu, G.; Liashenko, A.; Piskorz, P.; Komaromi, I.; Martin, R. L.; Fox, D. J.; Keith, T.; Al-Laham, M. A.; Peng, C. Y.; Nanayakkara, A.; Challacombe, M.; Gill, P. M. W.; Johnson, B.; Chen, W.; Wong, M. W.; Gonzalez, C.; Pople, J. A. 2003.